Journal Pre-proof

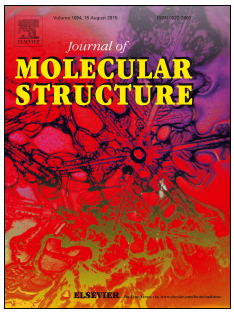

Study the solvation effect on 6-phenyl-2-thioxo-1,2-dihydropyridine-3-carbonitrile derivatives by TD- DFT calculations and molecular dynamics simulations

Mahmoud K. Abdel-Latif, H.R. Abd El-Mageed, Hussein S. Mohamed, F.M. Mustafa

PII: S0022-2860(19)31156-1

DOI: https://doi.org/10.1016/j.molstruc.2019.127056

Reference: MOLSTR 127056

To appear in: *Journal of Molecular Structure*

Received Date: 23 July 2019

Revised Date: 9 September 2019

Accepted Date: 9 September 2019

Please cite this article as: M.K. Abdel-Latif, H.R. Abd El-Mageed, H.S. Mohamed, F.M. Mustafa, Study the solvation effect on 6-phenyl-2-thioxo-1,2-dihydropyridine-3-carbonitrile derivatives by TD- DFT calculations and molecular dynamics simulations, *Journal of Molecular Structure* (2019), doi: https://doi.org/10.1016/j.molstruc.2019.127056.

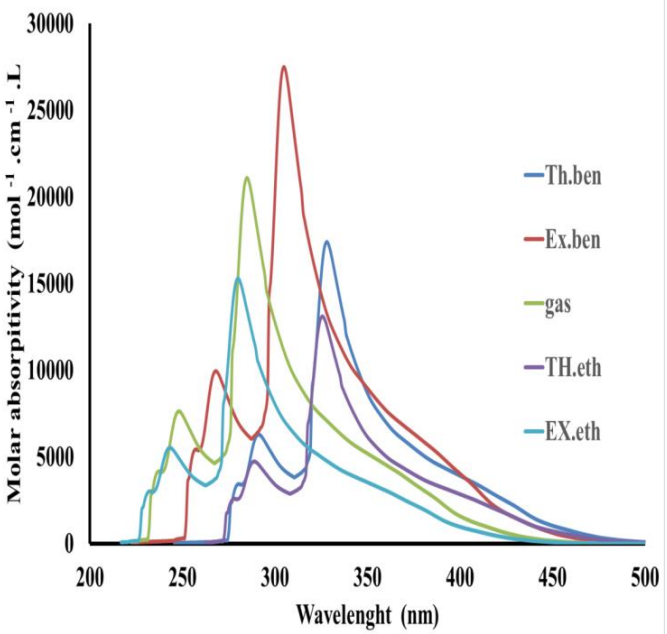

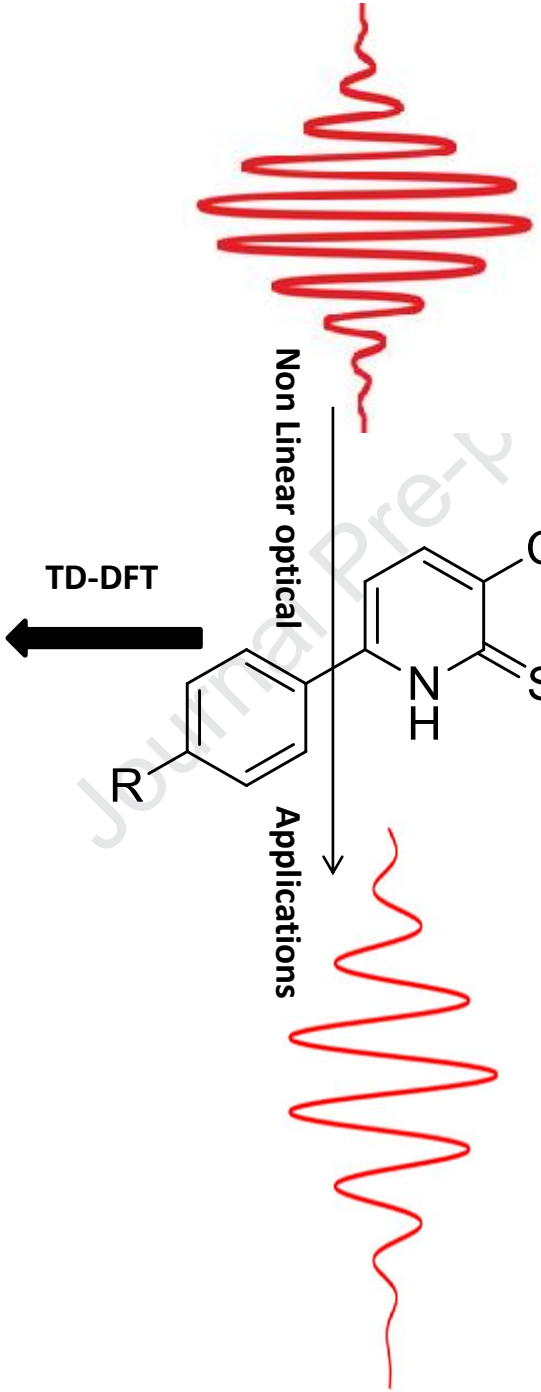

MD

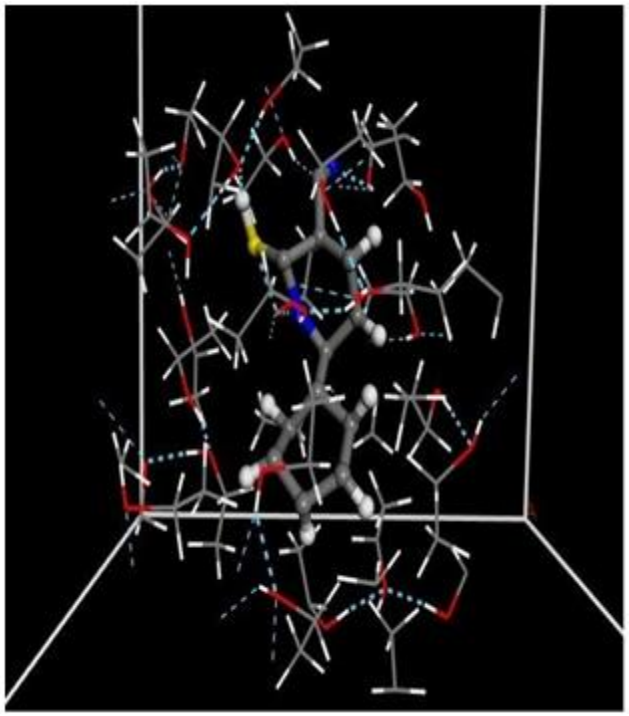

Study the solvation effect on 6-phenyl-2-thioxo-1,2-dihydropyridine-3-carbonitrile Derivatives by TD- DFT calculations and molecular dynamics simulations

Mahmoud K. Abdel-Latif*[a], H.R. Abd El-Mageed[b],Hussein S. Mohamed[c] and F. M. Mustafa[a].

[a]*Chemistry Department, Faculty of Science, Beni-Suef university, Beni-Suef City, Egypt.*
[b]Micro-analysis and environmental research and community services center, Faculty of Science, Beni-Suef university, Beni-Suef City, Egypt.
[c]*Research Institute of Medicinal and Aromatic Plants (RIMAP), Beni-Suef university, Beni-Suef City, Egypt.*
**Corresponding author mahmoud.abdellatif@science.bsu.edu.eg (Tel.:+201156634469)*

Abstract

The electronic structure of **6-phenyl-2-thioxo-1,2-dihydropyridine-3-carbonitrile** (2-mercapto-6-phenylpyridine-3-carbonitrile) and its some derivatives have been studied both theoretically and experimentally. The choice of these compounds was motivated by their biological importance and relevance. The corresponding proposed structures of all studied derivatives in this work were confirmed by FT-IR spectrophotometer, ^{1}HNMR spectra and XRD patterns. The Density Functional Theory (DFT) has been used to investigate the effect of substituents with different strengths of all studied compounds on the geometry structures, natural bond orbital (NBO) properties, electrostatic potential (ESP) and the global properties such as (the chemical hardness (η), global softness (S), and electronegativity (χ) by analysis of the charge distribution and extent of charge transfer in the molecule in the gas phase. Non-linear optical properties (NLO) such as (static dipole moment (μ), polarizability (α), anisotropy polarizability (Δα), first order hyperpolarizability (β) and mean second order hyperpolarizability (γ)) also, were computed by DFT in the gas and solvent (benzene and ethanol) phases. The effect of the different substitutions and solvent polarity on the NLO properties were also investigated to show their ability to be used as NLO compounds. We find that all studied compounds exhibited higher NLO properties compared to urea (reference materials) in the gas phase and showed higher NLO properties in ethanol than in the benzene phase. The effect of solvent polarity on the electronic absorption spectra of the studied molecules was measured experimentally and calculated theoretically at the Time-Dependent Density Functional Theory (TD-DFT) level of theory. The interactions of different solvents (ethanol and benzene) with studied compounds were also studied by molecular dynamics (MD) simulations. The radial distribution functions (RDFs) and coordination numbers (CNs) of all studied compounds in the different solvent are computed. The diffusion

coefficient (D) also was calculated to investigate the influence of substitutions on the mobility of the studied compounds in the surrounding solvent.

Key words: 6-phenyl-2-thioxo-1,2-dihydropyridine-3-carbonitrile, TD-DFT, MD simulations, NLO, Diffusion coefficient

Introduction

In the last decades, pyridine-2-thiol derivatives are employed in various biological applications such as anti-inflammatory, anti-tumor, ant mycobacterial, antifungal and antiviral activities [1–3]. The cytotoxicity of pyridine derivatives against several human cancer cell lines was reported [4-6]. Pyridin-2-thione derivatives represent useful synthetic intermediates for the synthesis of biologically active deazafolates ring systems, pyrimidine nucleosides, which reported to be significantly active both in vitro and vivo [7] and inhibitor of dihydrofolatereductase [8]. Furthermore, pyrimidine nucleosides are currently used dye to their cytotoxicity against various tumors as potentially as methotrexate [9,10] and the most effective antimetabolites currently employed in the treatment of different solid tumors [11]. Synthesis and anti-tumor activities of some new pyridines and pyrazolo [1, 5-a] pyrimidines were discussed [12]. The molecular structure of 3-(2-Mercaptopyridine)phthalonitrile was studied by computational and experimental approaches, the electronic absorption spectra, nonlinear optical properties, molecular electrostatic potential, and thermodynamic properties also were studied and reported [13]. Theoretical density functional and *ab initio* computational study of vertical ionization potentials, dipole moments and ^{13}C and ^{14}NNMR shifts of the 2-mercaptopyridine system was studied and reported [14].The solvent effects on the tautomerism and electronic absorption spectra of 3-Hydroxy-2-mercaptopyridine and 2,3-Dihydroxypyridine was studied [15]. The gas phase and solvent dependent preference of the tautomerization between 2-pyridinethiol and 2-pyridinethione had been assessed using variable temperature Fourier transform infrared (FTIR) experiments, and DFT computations [16].
Because of their wide range of biological activities and scientific relevance, 2-mercapto-6-phenylpyridine-3-carbonitrile and its derivatives are currently represented the subject of various investigations to explore a wide range of biological applications. Also, there is no any theoretical and computational study on these compounds under considerations. That’s why, the aim of the present work is to facilitate these biological investigations via the compilation of various physical electronic and structural parameters which would certainly underlie their biological activity using density functional theory. In addition to the NLO parameters and the solvent effect on them are also investigated in this work. The corresponding proposed structures of all studied compounds in this work are confirmed by FT-IR spectrophotometer, ^{1}HNMR spectra and XRD patterns as shown in the experimental part. Electronic absorption spectra of all studied compounds were computed

by TD-DFT method in Benzene and Ethanol solvents in addition to the gas phase. Molecular dynamical simulations is a strong tool to investigate the types of interaction between 2-thioxo-1,2-dihydropyridine-3-carbonitrile compound and the solvents as done by M.E. Salem et al [17]. Computational pharmacokinetic characterization of drug-likeness has been done for Ethyl pyridine substituted 3-cyanothiopheneo complexes using molecular dynamic simulation on the basis of an average root mean square deviation (RMSD) and radial distribution function (RDF) [18]. So, in this study we have used the MD simulations to gain more insight into the stability of these compounds in different solvents (ethanol and benzene) and their binding ways with the solvents using (RMSD) and (RDF).

2. Experimental Part

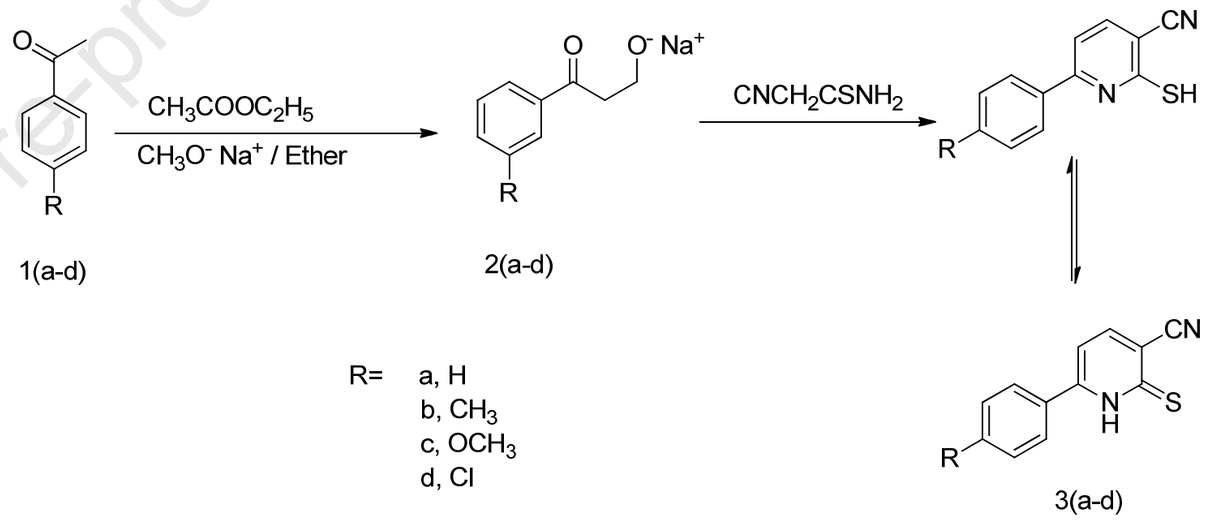

Scheme (1)

2.1 Instrumentation

All melting points are uncorrected. IR spectra were obtained (KBr disk) by using a Perkin Elmer 11650 FT-IR spectrophotometer. ^{1}HNMR spectra were recorded in $CDCl_3$ on a Varian mercury VXR-300 (300 MHz for 1H and 75 MHz for 13C). X-ray diffraction (XRD) patterns of the studied compounds were characterized with the help of Pananlytical Empryan Xray diffractometer 202 964 (the Netherlands). The scan range

was 5°–140. The electronic absorption spectra were measured on a Perkin Elmer Lambda 4B spectrophotometer using 1.0 cm fused quartz cells, where the spectrometer records linearly the percent of transmittance over the range 200-700 nm. Analytical data were carried out at Beni-Suef University. Polar (ethanol) and non-polar (benzene) solvents used in the present work were obtained from Merck, AR grade and used without further purification.

2.2 Synthesis:

Sodium 3-oxo-3-Arylpropan-1-olate (2):-

In a three necked flask containing [0.01 mol] of sodium methoxide and 20 ml ether, [0.01 mol] Actophenone derivatives **1** with [0.01 mol] ethyl formate was poured over it through separating funnel with efficient stirring. The solid product was collected at the pump and used directly in the reactions.

General procedure for the synthesis of compounds 3(a-d):-

A solution of (0.01 mol) sodium salt of compounds **2**, (0.01 mol) 2-Cyanoethanethioamide and piperidine acetate (1 ml) in H_2O (3 ml) was heated for 15 minutes. Acetic acid (1.5 ml) was added to the hot solution. The solid product was filtered off and recrystallized.

3a: 6-phenyl-2-thioxo-1,2-dihydropyridine-3-carbonitrile.

Red (yield 59%), m. p. 179-182^{o}C (Acetic acid), umax / cm^{-1} (KBr) 3350 (NH), 2229 (CN),1617(C=N). ^{1}HNMR (DMSO) d = 6.98-8.1 (m, 7H, aromatic protons),d = 13.3 (s, 1H, NH pyridine),. m/z 212 (Calcd for $C_{12}H_8N_2S$: C, 67.9; H, 3.8; N, 13.20; S, 15.1%. Found: C, 67.6; H, 3.9; N, 13.5; S, 14.9%.

3b: 2-thioxo-6-(p-tolyl)-1,2-dihydropyridine-3-carbonitrile.

Deep red (yield 68%), m. p. 190-195^{o}C (Acetic acid), umax / cm^{-1} (KBr) 3368 (NH), 2230 (CN),1634(C=N). ^{1}HNMR (DMSO) d= 1.82 (s, 3H, CH_3), d = 7.09-8.19 (m, 6H, aromatic protons),d = 12.6 (s, 1H, NH pyridine),. m/z 226 (Calcd for $C_{13}H_{10}N_2S$: C, 69; H, 4.45; N, 12.38; S, 14.17%. Found: C, 68.7; H, 4.49; N, 12.4; S, 14.14%.

3c: 6-(4-methoxyphenyl)-2-thioxo-1,2-dihydropyridine-3-carbonitrile.

Deep red (yield 63%), m. p. 210-215^{o}C (Dioxane), umax / cm^{-1} (KBr) 3344 (NH), 2229 (CN),1642(C=N), 1165 (C-O). ^{1}HNMR (DMSO) d= 3.76 (s, 3H, OCH3), d = 6.90-8.22 (m, 6H, aromatic protons), d = 13.33 (s, 1H, NH pyridine),. m/z 242 (Calcd for

$C_{13}H_{10}N_2OS$: C, 64.44; H, 4.16; N, 11.56; O, 6.6; S, 13.23%. Found: C, 64.47; H, 4.12; N, 11.59; O, 6.63; S, 13.20%.

3d: 6-(4-chlorophenyl)-2-thioxo-1,2-dihydropyridine-3-carbonitrile.

Orange (yield 72%), m. p. 225-227^{o}C (Dioxane), umax / cm^{-1} (KBr) 3315 (NH), 2223 (CN),1637(C=N). ^{1}HNMR (DMSO) d = 7.22-8.16 (m, 6H, aromatic protons), d = 13.20 (s, 1H, NH pyridine),. m/z 246 (Calcd for $C_{13}H_{10}N_2Cl$: C, 58.42; H, 2.86; N, 11.35; S, 12.99; Cl, 14.37%. Found: C, 58.45; H, 2.83; N, 11.38; S, 12.95; Cl, 14.39%.

FTIR and ^{1}HNMR spectra are presented in the supporting information in Figure S1 and S2 respectively. All characteristic peaks of FTIR and ^{1}HNMR of 3(a-d) compound are in good agreement with the previous studies [19,20]

X-ray diffraction patterns

The XRD of all studied compounds are given in Figure 1. All studied compound have semi-crystalline structures as shown in Figure 1. It is clear also from this Figure that, All compound have the X-ray diffraction peaks of mercaptophenylpyridine at typical scanning angles 2θ = 22.14, 25.18, 35.28, 38.34 [21], in addition to these peaks, there are two peaks appear (at 2θ = 13.00 and 45.23) in compounds 3a and 3b and disappear in compounds 3c and 3d also, in compound 3c there are an additionally peak appear at 2θ = 15.65. All characteristic peaks are appeared for all compounds but with different intensity. Compound 3c have the highest intensity compared to other compounds. The increasing in the intensity indicated that the enhancement in the degree of crystallinity. The degree of crystallinity can be calculated by separating intensities due to the amorphous and crystalline phase of the diffraction pattern. Percentage of crystallinity (Xc, %) is measured as the ratio of the crystalline area to total area according to the following equation [22].

$$\mathbf{Xc\ (\%) = \left[\frac{A_c}{A_a + A_c}\right] x\ 100\%} \quad \mathbf{(1)}$$

Where, Ac = area of the crystalline phase and Aa = area of the amorphous phase. The degree of crystallinity of compounds 3(a-d) are 68.44, 70.55, 75.65, and 72.52 % respectively. All the previous data confirmed that the corresponding proposed structures, of all studied compounds.

3- Computational details

Quantum mechanical calculations based on DFT were performed for all studies compounds using the Gaussian 09 program [23]. The Becke's three parameter Lee-Yang-Parr hybrid exchange-correlation (B3LYP) functional was used throughout this work [24-

27]. Full geometry optimization was performed using 6-311++G(d,p) as a basis set to generate the optimized structures and ground state properties of all studied compounds in the gas phase. Frequency calculation has been done at the same level of theory for the confirmation of the global minima. The electronic transition properties such as the maximum excitation wavelength **(λ_{max})** and oscillator strengths (f) were computed using TD-DFT [28] in the gas phase and different solvents adopting SCRF method, where the Polarizable Continuum Model (PCM) using the integral equation formalism variant (IEFPCM) is the default SCRF method [29-33]. MD simulations were performed using FORCITE Module, which is implemented in the Materials Studio 7 package [34] with the Condensed-Phase Optimized Molecular Potential for Atomistic simulation studies (COMPASS) force field [35–37]. All atoms were considered explicitly in a cubic box under a periodic boundary condition. This box contained 200 ethanol or benzene molecules and one unite from studied compounds. MD simulations were carried out under isothermal–isobaric (NPT) conditions, with pressure and temperature held at 1 atm and 300 K, respectively, by employing a Nose thermostat and Berendsen barostat. The equations of motion were integrated with the velocity Verlet algorithm for a total simulation time of 1 ns with a time step of 1 fs. During the simulations the non-bonded energies were calculated using the popular E_{wald} summation while the COMPASS force field was used to calculate both van der Waals and electrostatic interactions.

4- Results and Discussion

4.1 Energetic of the ground state

The full geometry optimizations of the proposed molecules were computed at the B3LYP/ 6-311++G(d,p) are shown in Figure 2. The different basis set is used to choose the one that reproduces values which are in the good agreement with experimental values obtained from the X-ray structure as shown next in Table S1 (S mean supporting information). The total energies, corresponding zero point vibrations energy (ZPVE) corrections, thermodynamics parameters and Dipole moment (D.M) of the studied compounds are listed in Table 1. The ZPE of the compound 3a is 0.1664 au which is increased to 0.1985 au upon substitution of the H-atom with methoxy group as an electron donating group. While the substitution of the H-atom with chloride group as an electron withdrawing decreases the ZBE to 0.1567 au. This means that the electron withdrawing groups stabilize the compounds in contrast to the electron donating groups (take into accounts that the methoxy and Cl are near of the same molecular weight).

4.2 Global descriptors Properties

The energies of High occupied molecular orbital (HOMO), low unoccupied molecular orbital (LUMO), energy gap (Eg) and the global properties of all studied compounds are

listed in Table 2. It is obvious that the separated phenylpridine ring is almost planar. The ionization energy value, I (-EHOMO), calculates the donating property of the molecule. The order of decreasing the ionization energy (increasing the oxidation power) of the proposed molecules, is 3c > 3b > 3a > 3d as shown in Table 2. The electron affinity value, A (-ELUMO), calculates the accepting property (reduction power) of the molecule. Analysis of A indicates that the order of decreasing the reduction power is: 3d >3a > 3b > 3c which is the opposite of the order of oxidation power. Eg is the gap between E_{HOMO} and E_{LUMO}; it measures the facile electron transition from HOMO to LUMO, this value can be displayed as the chemical reactivity of the molecules. Eg values in Table 2 show that the reactivity of these molecules increases in the order: 3c > 3d > 3b >3a. The dipole moment signifies the polarizability of the molecules. The values of dipole moments indicated that the order of the decrease the polarizability is: 3c > 3b > 3a > 3d which is of the same order of the oxidation power (c.f. Table 2). The global properties such as the global hardness η, electronegativity χ, electrostatic potential V and global softness S are calculated by the thesis equations [38]:

$$\eta = \frac{I - A}{2} \quad (2)$$

$$\chi = \frac{I + A}{2} \quad (3)$$

$$V = \frac{-(I + A)}{2} \quad (4)$$

$$S = \frac{1}{2\eta} \quad (5)$$

For any two molecules, the electron will be partially transferred from one the molecule which has low χ to that of high χ. The results show that the orders of decreasing χ (increasing charge transfer within the molecules) are: 3d >3a > 3b > 3c. The small η values for the studied compounds indicated that the ability of charge transfer inside the molecule. Therefore, the order of increasing of η is 3c > 3d > 3b >3a. There is a relationship between η and E_g as shown in Table 2. In which, the higher η values, the harder is the molecule and vice versa. The occupied and unoccupied molecular orbitals for the studied compounds are shown in Figure 3.

4.2. NBO analysis (used in the spectra part)

Natural atomic charge distributions based on Natural population analysis (NPA) was performed on the global minimum structure of compound 3a in the gas phase. The atomic charge distributions of all atoms in this compound are shown in Figure S3. The NBO's second-order perturbation theory and its second-order perturbation stabilization energy $E^{(2)}$ analysis describe the interaction between the idealized Lewis structure and the empty non-Lewis orbital as well as. The intramolecular, intermolecular bonding and bond interaction can be investigated by NBO analysis [39]. The larger value of $E^{(2)}$ value, indicated that more intensive in the interaction between electron donors and electron acceptors (more donating tendency from electron donors to electron acceptors). The

hyper conjugative interaction energy was derived from the second-order perturbation theory. For each donor NBO (i) and acceptor NBO (j), the stabilization energy $E^{(2)}$ associated with delocalization is estimated from the following equation [40]:

$$\mathbf{E^{(2)} = \Delta E_{ij} = q_i F (i, j)^2 / (\varepsilon_i - \varepsilon_j)} \qquad \mathbf{(6)}$$

Where q_i is the donor orbital occupancy, ε_j and ε_i the diagonal elements and F (i,j) is the off diagonal NBO Fock matrix element. The calculated charge transfer energy $E^{(2)}$ between the donor-acceptor orbital's of the studied compounds computed at B3LYP/6-311++G (d,p) level theory are summarized in Table 3, we find that the charges are transferred from σ (BD) to σ^* (BD)* orbitals with high stabilization energy $E^{(2)}$ in the most interaction.

4.3. NLO properties

Recently, NLO materials are at the forefront of current research due to their importance in providing the key functions of frequency shifting, optical modulation, optical switching, optical logic, and optical memory. So, we can use NLO materials in a large number of application such as modern communication technology, data storage, optical signal processing, and optical interconnections [41-44]. In this study, we computed NLO properties such as the total static dipole moment **(μ),** linear polarizability **(α)**, first hyperpolarizability tensor components **(β)** and mean second order hyperpolarizability **(γ)** of the molecules of the all studied compounds in gas, ethanol and benzene phases at B3LYP/6-311++G(d,p) level theory as shown in Tables S2-S4, respectively. All equations used in the calculations of NLO properties of the studied compound are listed in supporting information equations 7-11. Urea is one of the prototypical molecules used in the study of the NLO properties of molecular systems. Therefore it was used frequently as a threshold value for comparative purposes [45]. In this work, we chose as reference material because there were no experimental values of the NLO properties of the studied compounds. The magnitude of β is one of the key factors in the NLO system. The analysis of β computed theoretically for the studied compounds show that of the compound 3a (X=H) is 3 times higher than that of urea, while those of the derivatives; X=CH_3, OCH_3, and Cl are 4, 6, 3 higher than the reference Urea respectively in the gas phase as shown in Table S2. We also find that **β** and **γ** of these compounds increasing in ethanol phase as shown in Table S3 are larger than that in benzene as shown in Table S4. Therefore, the studied compounds are considered as effective candidates for NLO materials.

4.5 Electronic absorption spectra

The electronic absorption spectra of 2-mercapto-6-phenylpyridine-3-carbonitrile compound 3a and its derivatives 3b, 3c, 3d studied in this work depend on the type and extent of interaction between different moieties. Two possible types of interaction between subsystems can exist, as shown in scheme 2. For example, (i) no interaction between phenylpyridine and the terminal phenyl group Ph-X (ii) full conjugation between the two subsystems Ph-X and phenylpyridine.

4.5.1 Electronic absorption spectra of 3a.

The results of the experimental and theoretical electronic absorption spectra of compound 3a in ethanol and benzene are presented in Figure 4. The experimental spectrum in both solvents is composed of two spectral bands in the range 200-500 nm. In benzene, the experimental UV spectrum shows two intense bands at 269.0 nm and 306.0 nm. Increasing solvent polarity from benzene to ethanol results in a blue shift of the two bands, where the first band is shifted to 245.0 nm and the second band is shifted to 281.0 nm, respectively. Furthermore, increasing solvent polarity causes a marked decrease in the intensity of the two bands going from Benzene to Ethanol. TD/B3LYP/6-311++G(d,p) level theory calculation is valuable for the analysis of the experimental UV Spectra of compound 3a in different solvents. The theoretical calculations are in good agreement with the experimental calculations. Since increasing the solvent polarity from Benzene to Ethanol has the same trend of decreasing of the intensity. In addition to the blue shift which noticed experimentally by increasing the solvent polarity. The theoretically calculated spectra showed a λmax of 326.87 nm for the first band in Ethanol, and for the first band 329.43 (S1) in Benzene, and as shown in Table 5. The two observed spectral bands are assigned as (π-π*) transitions, as reflected from the values of molar absorptivity (ε = 5000-30000). Predicting and assigning the origin of the experimental spectrum of compound 3a, requires the calculations of the theoretical gas phase transitions of the various subsystems a, b, c, and d using TD-B3LYP/6-311++G(d,p) level of theory, which are presented in Figure 5. Three strong transitions are computed at 292.0, 261.0, and 239.0 nm for subsystem a; three transitions are computed at 274.0, 260.0, and 245.0 nm for subsystem b; three transitions are computed at 308.0, 285.0, and 254.0 nm for subsystem c; three transitions are computed at 298.0, 292.0, and 282.0 nm for d; three transitions are computed at 326.0, 292.0, and 284.0 nm for compound 3a. The correlation of the theoretical transitions of Table 4 between the various subsystems shows that the transition at 292.0 nm of subsystem d correlates with the transition at 292.0 nm of compound 3a. Moreover, the transition at 282.0 nm of subsystem d correlates with that at 284.0 nm of compound 3a. It is clear that from this division, the pyridine rings with the CN and SH groups contribute the most of the two spectral bands of the gas phase of compound 3a. This is confirmed by the charge density of HOMO of compound 3a, where the charge density is localized on this moiety. The

delocalization of the charge density of the HOMO over the whole molecule of compounds 3b, 3c, and 3d is increased upon substitution in the para position of the phenyl ring.

4.5.2 Electronic absorption spectra of 3b.

Compound 3b results by inserting CH_3 group in the position X in Ph-X of compound 3a. The experimental and theoretical electronic absorption spectra of compound 3b in benzene and ethanol are combined and shown in Figure 6 and Table 6. In benzene, the experimental spectrum is composed of two bands, at 338.0 nm and 307.0 nm. Increasing solvent polarity from Benzene to Ethanol results in a blue shift of the two bands, where the first band is shifted to 336.0 nm and the second band is shifted to 305.0 nm, respectively. Furthermore, increasing solvent polarity causes a marked decrease in the intensity of both bands. The two observed bands are assigned as (π-π^*) transitions, based on the values of molar absorptive (ε = 5000-30.000). The interpretation of the experimentally observed UV Spectra of compound 3b in Benzene and Ethanol requires the theoretical calculations of the vertical transitions using TD/ B3LYP/6-311++G(d,p) level theory. Recorded theoretical spectra are in agreement with the experiment since the blue shift and the decreasing intensity are observed with increasing the solvent polarity. TD/DFT showed the λ_{max} of 332.45 nm (S1) and 301.79 nm (S2) with respect to Benzene and 330.49 nm (S1) and 300.39 nm (S2) in Ethanol.

4.5.3 Electronic absorption spectra of 3c.

Compound 3c results by inserting OCH_3 group in the position X of compound 3a. The experimental and theoretical electronic absorption spectra of compound 3c in Benzene and Ethanol are shown in Figure 7 and Table 7. The experimental spectrum in Benzene is composed of two bands at 348.0 nm and 277.0 nm. The change of solvent polarity from Benzene to Ethanol results in a small red shift by 1 nm of the first band, where the second band is blue shifted by 1 nm. Additionally, increasing solvent polarity causes a marked decrease in the intensity of the two bands. The values of molar absorptivity (ε = 5000-30000) indicate that the two observed bands have π-π^* character. The theoretical vertical transitions using TD/ B3LYP/6-311++G(d,p) level theory is valuable for the analysis of the experimental UV Spectra of 3 which gives values for λ_{max} of 346.03 nm (S1) for the first band in Benzene , and for the first band 345.15 (S1) in Ethanol , and as shown in Table 6.

4.5.4 Electronic absorption spectra of 3d.

Compound 3d results by inserting Cl group in the position X of compound 3a. The experimental and theoretical electronic absorption spectra of compound 3d in Benzene and Ethanol are shown in Figure 8 and Table 8. The experimental spectrum in Benzene is composed of three bands. The experimental UV spectrum in benzene shows two intense bands at 284.0 nm and 310.0 nm. Increasing solvent polarity from benzene to ethanol results in a blue shift of the two bands, where the first band is shifted to 270.0 nm and the second band is shifted to 298.0 nm, respectively. These transitions are assigned to π-π* transition as indicated by the molar absorptivity values (ε=5000-30000). The theoretical electronic absorption spectra using TD/ B3LYP/6-311++G(d,p) level theory is valuable for the analysis of the experimental UV Spectra of compound 3d. The calculated spectra showed a blue shift by switching the solvent from Benzene to Ethanol. In benzene, the values of λ_{max} is at 340.22 nm for (S1) and 278.2 nm for (S2), while the λ_{max} is at 334.44 for (S1) and 270.31 nm for (S2) in Ethanol as shown in Table 8.

4.6 Molecular Electrostatic potential (MEP)

The MEP is related to the electronic density and is a very useful descriptor in determining the sites for electrophilic and nucleophilic reactions as well as hydrogen bonding interactions. To predict reactive sites for electrophilic and nucleophilic attack for the studied compounds, the MEP at the B3LYP/6-311++G(d,p) level of theory was calculated. The negative (red and yellow) regions of the MEP are related to electrophilic reactivity and the positive (blue) regions are related to nucleophilic reactivity, as indiicated in Figure 9. It is clear that from Figure 9, the MEP of compound 3a displayed all atoms with positive electron densities (sites for nucleophilic attack) except the nitrogen atom in (CN) group which showed a negative electron density (sites for electrophilic attack). For compound 3b, all atoms have a positive electron densities except the nitrogen atom in (CN) group has a negative electron density and the sulfur atom in (SH) group displayed an intermediate negative electron density. Compound 3c, showed all atoms with a positive electron densities except the nitrogen and the oxygen atoms in (CN) and (OCH3) groups respectively where they showed negative electron density while the sulfur atom in (SH) group displayed an intermediate negative electron density. In the compound 3d all atoms displayed with a positive electron densities but the nitrogen atom in (CN) group displayed with a negative electron density. The sulfur atom in (SH) group and the chloride atom displayed with an intermediate negative electron density. The MEP map displayed that the negative potential sites were on electronegative atoms (N, O and S) and the positive potential sites were around the hydrogen atoms. These sites give information and some light on the regions that the compound can have intermolecular interactions with others.

4.7 MD simulations

To get more insight on the interaction between the studied compounds and different solvent such as ethanol and benzene. MD simulations can be used to calculate diffusion coefficient and study the hydrogen bonds (HBs) forming between the studied compounds and different solvents. Figures S4 and S5 show MD snapshots of all studied compounds in ethanol and benzene respectively. All snapshots were taken at 1nm (all snapshots are taken within 3Å from the studied compounds) in which the green dashed line showed HBs formation between studied compounds and solvents. It has been found that from Figures S4 and S5 all studied compounds formed hydrogen bond with ethanol through S, N and H atoms (studied compounds). The HBs formation between all studied compounds + ethanol and all studied compounds + benzene can be explored by the radial distribution functions (RDFs) and coordination numbers (CNs). The RDF is the probability of finding particle "B" within the range (r+dr) around particle A, and expressed as gAB(r). The CN is obtained by integrating the gAB(r) [46]. The RDFs for HB sites of the parent and the methoxy compounds with the oxygen (O) or hydrogen (H) atoms of ethanol and with hydrogen (H) atoms of benzene molecules are plotted in Figure 10, together with the corresponding coordination numbers (CNs).

4.7.1 RDFs and CNs of all compounds in ethanol and benzene

4.7.1.1. Compound 3a

The RDF of the hydrogen atoms of the SH group of the parent with O atom of ethanol as shown in Figure 10 (1a), $HS_{(parent)}\cdots\cdots O_{(ethanol)}$, has an intense peak at 2.4 Å which is related to the HBs formation; since it is within the HB distance (2.5 Å). The S and N atoms of the parent compound formed also HBs with the hydrogen atoms of ethanol $S_{(parent)}\cdots\cdots H_{(ethanol)}$ and $N_{(parent)}\cdots\cdots H_{(ethanol)}$ have intensive peaks at 1.8 and 2.4 Å respectively and the intensity of the former peak is greater than the later one as shown in Figure 10 (1b and 1c), indicating that the HB of the former is stronger than the later one. The S and N atoms of the parent compound also formed HBs with the hydrogen atoms of benzene $S_{(parent)}\cdots\cdots H_{(benzene)}$ and $N_{(parent)}\cdots\cdots H_{(benzene)}$ have intensive peaks at 2.4 and 1.5 Å respectively and intensity of the later peak is greater than the former as shown in Figure 10 (1d and 1f), indicating the HB of the later is stronger than the former one, in addition to four peaks with small intensity are found at former due to nonbonding interactions. Parent compound strongly formed HBs with ethanol and benzene especially in $S_{(parent)}\cdots\cdots H_{(ethanol)}$ and $N_{(parent)}\cdots\cdots H_{(benzene)}$ according to RDFs and CNs.

4.7.1.2. Compound 3b

The RDF of the hydrogen atoms of the SH group of CH_3 with O atom of ethanol shown in Figure S6 (2a). The $HS_{(CH3)}\cdots\cdots O_{(ethanol)}$, has an intense peak at 2.5 Å which is related to the HBs formation. The S and N atoms of the CH_3 compound formed also HBs with the hydrogen atoms of ethanol $S_{(CH3)}\cdots\cdots H_{(ethanol)}$ and $N_{(CH3)}\cdots\cdots H_{(ethanol)}$ and they have intensive peaks at 1.7 and 1.2 Å respectively. The intensity of the later peak is greater

than the former as shown in Figure S6 (2b and 2c), indicating that the HB of the later is stronger than the former one. In addition, the former one has five peaks with low intensity due to nonbonding interactions. The S and N atoms of the parent compound formed also HBs with the hydrogen atoms of benzene $S_{(CH3)}\cdots\cdots H_{(benzene)}$ and $N_{(CH3)}\cdots\cdots H_{(benzene)}$ have intensive peaks at 2.3 and 1.4 Å respectively and intensity of the later peak is greater than the former as shown in Figure S6 (2d and 2f), indicating the HB of the later is stronger than the former one. CH_3 compound strongly formed HBs with ethanol and benzene especially at $N_{(CH3)}\cdots\cdots H_{(ethanol)}$ and $N_{(CH3)}\cdots\cdots H_{(benzene)}$ centers according to RDFs and CNs parameters.

4.7.1.3. Compound 3c

The RDF of the hydrogen atoms of the SH group of OCH_3 compound with O atom of ethanol as shown in Figure S7 (3a), $HS_{(OCH3)}\cdots\cdots O_{(ethanol)}$, has an intense peak at 2.3 Å which is related to the HBs formation. The S and N atoms of the parent compound formed also HBs with the hydrogen atoms of ethanol $S_{(OCH3)}\cdots\cdots H_{(ethanol)}$ and $N_{(OCH3)}\cdots\cdots H_{(ethanol)}$ with the same intensive peaks at 1.7 as shown in Figure S7 (3b and 3c). The HB of the former one is stronger than the later one. The S and N atoms of the OCH_3 compound formed also HBs with the hydrogen atoms of benzene $S_{(OCH3)}\cdots\cdots H_{(benzene)}$ and $N_{(OCH3)}\cdots\cdots H_{(benzene)}$. These HBs have intensive peaks at 2.45 for the S atom and 1.6 Å for the N atom and intensity of the later peak is greater than the former one as shown in Figure S7 (3d and 3f), indicating that the HB of the N atom is stronger than the S Atom, in addition to two peaks with small intensity are found at former due to nonbonding interactions. Also oxygen atom in OCH_3 group $O_{(OCH3)}\cdots\cdots H_{(ethanol)}$ formed HB with the hydrogen atoms of ethanol with highly intensive peak at 1.15 Å in addition to four peaks with low intensity due to nonbonding interactions as shown in Figure S7 (3g). So, OCH_3 compound strongly formed HBs with ethanol and benzene especially at S and O centers according to RDFs and CNs.

4.7.1.4. Compound 3d

The RDF of the hydrogen atoms of the SH group of Cl compound with O atom of ethanol shown in Figure S8 (4a), $HS_{(Cl)}\cdots\cdots O_{(ethanol)}$, has an intense peak at 2.3 Å which is related to the HBs formation. The S and N atoms of the Cl compound formed also HBs with the hydrogen atoms of ethanol $S_{(Cl)}\cdots\cdots H_{(ethanol)}$ and $N_{(Cl)}\cdots\cdots H_{(ethanol)}$ with intensive peaks at 1.6 and 1.5 Å respectively and the later peak is more intense than the former one as shown in Figure S8 (4b and 4c), indicating the strength HB formation of the later than the former one. Also the later one has additionally five peaks with low intensity due to nonbonding interactions. The S and N atoms of the Cl compound have also HBs peaks formation with the hydrogen atoms of benzene $S_{(Cl)}\cdots\cdots H_{(benzene)}$ and $N_{(Cl)}\cdots\cdots H_{(benzene)}$ at 2.4 and 1.5 Å respectively. And the intensity of the later peak is greater than the former

as shown in Figure S8 (4d and 4f), indicating the HB of the later is stronger than the former one. Cl compound strongly formed HBs with ethanol and benzene especially in at the N center ($N_{(Cl)}\cdots\cdots H_{(ethanol)}$ and $N_{(Cl)}\cdots\cdots H_{(benzene)}$) according to RDFs and CNs.

4.7.2 Diffusion coefficient (D)

The diffusion coefficient *D* is related to the slope of the mean square displacement of solvent molecules and can be calculated by the Einstein relation equation. When the solute molecules move faster in the solution the solute-solvent collisions increase and more thermal energy are generated, and as a result the diffusion coefficient increase. This indicated that solute which has lower value of D interact with solvent stronger than that has higher value of D [47]. Diffusion coefficient of all studied compounds in both ethanol and benzene are calculated by MD simulation and summarized in Table 9. The values of Diffusion coefficient of OCH_3 compound are the lowest values which indicated that the interaction between this compound and these solvent are the strongest with respect to the rest of compounds. Also the RDFs and the CNs calculations confirmed that this interaction is the strongest more HBs are formed. So, we can say that OCH_3 and CH_3 substitutions enhanced the interaction of Thiol with ethanol and benzene but Cl decreasing this interaction according to the diffusion coefficient values, RDFs and CNs.

Conclusion

The corresponding proposed structures of all studied derivatives in this work are confirmed by FT-IR spectrophotometer, ^{1}HNMR spectra and XRD patterns. Electronic structure and geometry optimization of 2-mercapto-6-phenylpyridine-3-carbonitrile compound 3a and some of its derivatives 3b-3d, are investigated theoretically at B3LYP/6-311++G(d,p) level theory. All the studied compounds are found to be planar. The ground state properties of compounds 3(a-d) show that compound 3c has the lowest E_{HOMO}, E_{LUMO}, and ΔE indicating highest reactivity. The Compound 3c is found to have the highest polarity, as shown from the computed dipole moment. The polarizability and hyperpolarizabilities parameters indicated that compounds under investigation are excellent candidates for NLO materials comparing the urea compound. Electronic absorption spectra are investigated experimentally in Benzene and Ethanol; and theoretically in gas phase at the TD-B3LYP/6-311++G(d,p) level of theory. Compounds 3b, 3c exhibit 2 bands each in the accessible vis-UV range investigated, while compounds 3a and 3d exhibit 3 bands each in both solvents. The band maxima (λ_{max}) and intensities of the spectra are found to have solvent dependence. The overall trend is the blue shift upon increasing the solvent polarity. It is noticed that decreasing of the band intensities going from Benzene as non-polar solvent to Ethanol as polar solvent. Theoretical calculations of the vertical excitations at the TD-B3LYP/6-311++G(d,p) level

theory reproduced the experimental spectra, indicating a good agreement between theory and experiment. Molecular dynamic simulations based on the RDFs, CNs and D parameters showed and confirmed that compounds 3b and 3c exhibits stronger interactions and formed many HBs with ethanol and benzene than compound 3a and 3d. Also, MD simulations confirmed that, the methoxy (OCH_3) compound (3c) has the stormiest interactions with the used solvents due to many hydrogen bonding formations.

References

1. F.M. Abdel-Megeid, Synthesis and antiviral evaluation of some new pyrazole and fused pyrazolopyrimidine derivatives, 16 (2008), 7102-7106.
2. F.V. Rocha, C.V. Barra, A.E. Mauro, I.Z. Carlos, L.N. ElGhozzi, A. Gautier, Laurent. Morel, Adelino. Vieira, Synthesis, Characterization, X-ray Structure, DNA Cleavage, and Cytotoxic Activities of Palladium(II) Complexes of 4-Phenyl-3-thiosemicarbazide and Triphenylphosphane, 25 (2013), 4499-4505.
3. M.Y. Shin, J.H. Han, H.S. Chung, In vivo effects of lead on erythrocytes following chronic exposure through drinking water, *29* (2006), 1158-1163.
4. A. Basnet, P. Thapa, R. Karki, Y. Jahng, B.S. Lee, 2, 4, 6-Trisubstituted pyridines: synthesis, topoisomerase I and II inhibitory activity, cytotoxicity, and structure–activity relationship, 15 (2007), 4351-4359.
5. S. Cesarini, A. Spallarossa, A. Ranise, S. Schenone, C. Rosano, P. Loddo. R. La Colla, N-Acylated and N, N′-diacylated imidazolidine-2-thione derivatives and N, N′-diacylated tetrahydropyrimidine-2 (1H)-thione analogues Synthesis and antiproliferative activity, 44 (2009), 1106-1118.
6. C.Jr. Temple, R.D. Elliott, J.A. Montgomery, Pyrido [2, 3-d] pyrimidines synthesis of the 5-deaza analogs of aminopterin, methotrexate, folic acid and N10-methylfolic acid, 47 (1982), 761-764.
7. A. Gangjee, K.A. Ohemeng, J.J. Tulachka, F.T. Lin, A.A. Katoh, Synthesis of some 2, 4-disubstituted tetrahydropyrimido [4, 5-b] quinolines as potential antitumor agents, 22 (1985), 1149-1151.
8. H.A. Naby, R. Mekheimer, A. Abd-Elhameed, K. Sadek, A convenient one-pot synthesis of pyrimido [4, 5-b] quinolines as 5-deaza non-classical antifolate inhibitors,11 (1999), 678-679.
9. N.M. Khalifa, M.M. Ramla, A.E. Amr, G.E. Abdulla, Synthesis and Anti-Inflammatory Activities of Some Novel S-Pyridyl Glycosides Derivatives, *183* (2008), 3046-3062.
10. E.C. Taylor, P.J. Harrington, S.R. Fletcher, G.P. Beardsley, R.G. Moran, Synthesis of the antileukemic agents 5, 10-dideazaaminopterin and 5, 10-dideaza-5, 6, 7, 8-tetrahydroaminopterin, 28 (1985), 914-921.
11. T.A. Farghaly, S.M. Gomha, E.M. Abbas, M.M. Abdalla, Hydrazonoyl Halides as Precursors for New Fused Heterocycles of 5α-Reductase Inhibitors, 345 (2012), 117-122.
12. H. Tanak, Y. Köysal, S. Işık, H. Yaman, V. Ahsen, Experimental and Computational Approaches to the Molecular Structure of 3-(2-Mercaptopyridine)phthalonitrile, 32 (2011), 673-680.

13. O.M. Ahmed, M.A. Mohamed, R.R. Ahmed, S.A. Ahmed, Synthesis and anti-tumor activities of some new pyridines and pyrazolo [1, 5-a] pyrimidines, *44* (2009), 3519-3523

14. V. Martinez, M.J. Gil, Theoretical density functional and ab initio computational study of vertical ionization potentials, dipole moments and 13 C and 14 N-NMR shifts of the 2-mercaptopyridine system A model for thiated nucleobases, 2 (1999), 33-38.

15. W. Yan, Y. Xue, H. Zhu, J. Zeng, D. Xie, A theoretical study of solvent effects on tautomerism and electronic absorption spectra of 3-hydroxy-2-mercaptopyridine and 2, 3-dihydroxypyridine, 25 (2004), 1833-1839.

16. D. Moran, K. Sukcharoenphon, R. Puchta, H.F. Schaefer, P.V.R. Schleyer, C.D. Hoff, 2-pyridinethiol/2-pyridinethione tautomeric equilibrium. A comparative experimental and computational study, 67 (2002), 9061-9069.

17. M.E. Salem, A.A. Ahmed, A.F. Darweesh, O. Kühn, A.H. Elwahy, Synthesis and DFT calculations of 2-thioxo-1, 2-dihydropyridine-3-carbonitrile as versatile precursors for novel pharmacophoric hybrid molecules, *1176* (2019), 19-30.

18. S. Ahmad, S. Raza, R. Uddin, S.S. Azam, Binding mode analysis, dynamic simulation and binding free energy calculations of the MurF ligase from Acinetobacter baumannii, 77 (2017), 72-85.

19. M.V. Castillo, J.L. Pergomet, G.A. Carnavale, L. Davies, J. Zinczuk, S.A. Brandán, FTIR, FT Raman, UV–Visible and NMR spectroscopic studies on 3, 3′, 4, 4′-tetrachloroazoxybenzene, an azoxybenzene derivative with toxic effects, 1142 (2017), 18-27.

20. D. Romani, María. J. Marquez, María. B. Marquez, Silvia. A. Brandan, Structural, topological and vibrational properties of an isothiazole derivatives series with antiviral activities, 1100 (2015), 279-289

21. R.A. Senthil, J. Theerthagiri, J. Madhavan, Optimization of performance characteristics of 2-mercaptopyridine-doped polyvinylidene fluoride (PVDF) polymer electrolytes for dye-sensitized solar cells, 406 (2014), 133-138.

22. H.R. Abd El-Mageed, H.M. Abd El-Salam, M.F. Eissa, Spectroscopic study on poly (acrylic acid-co-acrylamide)-graft–polyaniline as a radiation dosimeter for alpha particles, 178 (2017), 374-381.

23. Gaussian 09, Revision C.02, M. J. Frisch, G. W. Trucks, H. B. Schlegel, G. E. Scuseria, M. A. Robb, J. R. Cheeseman, J. A. Montgomery, Jr., T. Vreven, K. N. Kudin, J. C. Burant, J. M. Millam, S. S. Iyengar, J. Tomasi, V. Barone, B. Mennucci, M. Cossi, G. Scalmani, N. Rega, G. A. Petersson, H. Nakatsuji, M. Hada, M. Ehara, K. Toyota, R. Fukuda, J. Hasegawa, M. Ishida, T. Nakajima, Y. Honda, O. Kitao, H. Nakai, M. Klene, X. Li, J. E. Knox, H. P. Hratchian, J. B. Cross, V. Bakken, C. Adamo, J. Jaramillo, R. Gomperts, R. E. Stratmann, O. Yazyev, A. J. Austin, R. Cammi, C. Pomelli, J. W. Ochterski, P. Y. Ayala, K. Morokuma, G. A. Voth, P. Salvador, J. J. Dannenberg, V. G. Zakrzewski, S. Dapprich, A. D. Daniels, M. C. Strain, O. Farkas, D. K. Malick, A. D. Rabuck, K. Raghavachari, J. B. Foresman, J. V. Ortiz, Q. Cui, A. G. Baboul, S. Clifford, J. Cioslowski, B. B. Stefanov, G. Liu, A. Liashenko, P. Piskorz, I. Komaromi, R. L. Martin, D. J. Fox, T. Keith, M. A. Al-Laham, C. Y. Peng, A. Nanayakkara, M. Challacombe, P. M. W. Gill, B. Johnson, W. Chen, M. W. Wong, C. Gonzalez, and J. A. Pople, Gaussian, Inc., Wallingford CT, 2009.

24. A.D. Becke, Density-functional thermochemistry. IV. A new dynamical correlation functional and implications for exact-exchange mixing, *104* (1996), 1040-1046.

25. A.D. Becke, Density-functional thermochemistry. V. Systematic optimization of exchange-correlation functionals, *107* (1997), 8554-8560.

26. K. Raghavachari, G.W. Trucks, J.A. Pople, M. Head-Gordon, A fifth-order perturbation comparison of electron correlation theories, *57* (1989), 479-483.

27. A.D. Becke, A new mixing of Hartree–Fock and local density-functional theories, *98* (1993), 1372-1377.

28. L.D. Künne, Recent developments and applications of modern density functional theory, 204 (1998), 263-264.

29. T. Schaefer, T.A. Wildman, S.R. Salman, The perpendicular conformation of 2-hydroxythiophenol. Intramolecular hydrogen bonding to a specific lone pair, *10* (1980), 107-110.

30. T. Schaefer, S.R. Salman, T.A. Wildman, P.D. Clark, Conformational consequences of intramolecular hydrogen bonding by OH to the directional lone-pair of sulfur in derivatives of methyl phenyl sulfide, diphenyl sulfide, and diphenyl disulfide, *2* (1882), 342-348.

31. W. Kohn, A.D. Becke, R.G. Parr, Density functional theory of electronic structure, *31* (1996), 12974-12980.

32. S. Scrocco, J. E.Tomasi, Electrostatic interaction of a solute with a continuum. A direct utilizaion of Ab initio molecular potentials for the prevision of solvent effects, *55* (1981), 117-129.

33. J. Pitarch, V. Moliner, J.L. Pascual, E. Silla, I. Tuñón, Can hydrophobic interactions be correctly reproduced by the continuum models, *23* (1996), 9955-9959.

34. L.B. Poole, The basics of thiols and cysteines in redox biology and chemistry, *80* (2015), 148-157.

35. Accelrys Software Inc., Materials Studio Release Notes.

36. S.W. Bunte, H. Sun, Molecular modeling of energetic materials: the parameterization and validation of nitrate esters in the COMPASS force field, *104* (2000), 2477-2489.

37. H. Sun, P. Ren, J.R. Fried, The COMPASS force field: parameterization and validation for phosphazenes, *8* (1998), 229-246.

38. H. Sun, Ab initio calculations and force field development for computer simulation of polysilanes, *28* (1995), 701-712.

39. F. Weinhold, C. Landis, A Natural Bond Orbital Donor Acceptor Perspective, 1 (2005), Cambridge University Press.

40. A.E. Reed, F. Weinhold, Natural bond orbital analysis of near-Hartree–Fock water dimer, *6* (1983), 4066-4073.

41. A.J. Foster, F. Weinhold, Natural hybrid orbitals, *24* (1980), 7211-7218.

42. T. Pal, T. Kar, G. Bocelli, L. Rigi, Synthesis, growth, and characterization of L-arginine acetate crystal a potential NLO material, *3* (2003), 13-16.

43. S.R. Marder, J. E. Sohn, G.D. Stucky, Nonlinear optical properties of organic and polymeric materials, 35 (1983), 708-712.

44. D. S. Chemla, J. Zyss, Nonlinear Optical Properties of Organic Molecules and Crystals, 1 (2012), Elsevier.

45. P. N. Prasad, D. J. Williams, Introduction to Nonlinear Optical Effects in Molecules and Polymers, 1 (1990), Wiley, New York.

46. M. Arivanandhan, C. Sanjeeviraja, K. Sankaranarayanan, S.K. Das, G.K. Samanta, P.K. Datta, Growth of urea doped benzophenone single crystal for nonlinear optical applications, 28(2006), 324-330.

47. M. Meunier, Diffusion coefficients of small gas molecules in amorphous cis-1, 4-polybutadiene estimated by molecular dynamics simulations, 123 (2005), 134-136.

48. M. AlRefai1, Synthesis and characterization of new 3,5-disubstituted-4,5-dihydro-1H-pyrazole and their carbothioamide derivatives, 6 (2015), 78-83.

49. A.R. Katritzky, S. Rachwal, B. Rachwal, Recent progress in the synthesis of 1, 2, 3, 4,-tetrahydroquinolines, (1996), 15031-15070.

Table 1: The energetics, thermodynamics parameters, zero point energy corrections and dipole moment of the studied compounds, calculated at B3LYP/6-311++G(d,p) level.

G.S. Properties	1	2	3	4
E_0(au)	-969.94886	-1009.2771	-1084.507	-1429.5713
E_0 (Kcal/mol)	-608642.91	-633321.4	-680528.15	-897056
E_0 (KJ/mol)	-2546115.8	-2649352.5	-2846830.9	-3752624.7
E_{ZPE} (au)	0.166380	0.193445	0.198508	0.156683
H_{corr}(au)	0.178802	0.208747	0.213643	0.170366
G_{corr}(au)	0.126450	0.150374	0.154760	0.171311
$E_0 + E_{ZPE}$ (au)	-969.782480	-1009.08368	-1084.30850	-1429.41463
$E_0 + H_{corr}$ (au)	-969.769115	-1009.06838	-1084.29243	-1429.40000
$E_0 + G_{corr}$(au)	-969.822410	-1009.12675	-1084.35225	-1429.45680
Dipole Moment (D)	4.414	5.198	5.426	2.991

Table 2: Energies in (a.u.) of molecular orbitals, energy gap Eg (eV) and global properties for the studied compounds using B3LYP/6-31++G (d,p).

Orbitals	1	2	3	4
E_{HOMO} [a]	-0.24917	-0.24393	-0.2337	-0.2515
I,eV	6.777	6.635	6.357	6.841
E_{HOMO-1}	-0.26956	-0.26339	-0.25649	-o.26976
E_{LUMO} [b]	-0.09189	-0.08906	-0.08593	-0.0977
A, eV	2.499	2.422	2.336	2.657
E_{LUMO+1}	-0.05882	-0.05662	-0.05511	-0.06430
Eg, eV	4.28	4.21	4.02	4.18
χ,eV	4.638	4.529	4.357	4.749
V,eV	-4.638	-4.529	-4.357	-4.749
η,eV	2.139	2.107	2.011	2.092
S,eV^{-1}	0.2338	0.2373	0.2486	0.2390

[a] I.E. = - E_{HOMO} [b] E. A. = - E_{LUMO}

Table 3: Second Order Perturbation energy (E^2), analysis of Fock matrix of compound 1 at B3LYP/6-311++G(d,p).

Donor	ED (i) (e)	Acceptor	ED (i) (e)	$E^{(2)}$ (kcal/mol)	E(j)-E(i) (a.u)	F(i,j)c (a.u)
BD (2) C 1 - N 6	1.69282	BD*(2) C 4 - C 5	0.46182	31.11	0.3	0.089
BD (2) C 2 - C 3	1.6655	BD*(2) C 1 - N 6	0.41488	28.86	0.27	0.081
BD (2) C 2 - C 3	1.6655	BD*(2) C 4 - C 5	0.46182	15.84	0.26	0.06
BD (2) C 4 - C 5	1.61538	BD*(3) C 22 - N 23	0.0858	18.52	0.38	0.081
BD (2) C 9 - C 11	1.63638	BD*(2) C 1 - N 6	0.41488	18.71	0.25	0.062
BD (2) C 9 - C 11	1.63638	BD*(2) C 10 - C 12	0.29651	18.96	0.29	0.067
BD (2) C 9 - C 11	1.63638	BD*(2) C 14 - C 16	0.32885	19.65	0.28	0.067
BD (2) C 10 - C 12	1.65248	BD*(2) C 9 - C 11	0.3772	19.94	0.28	0.067
BD (2) C 10 - C 12	1.65248	BD*(2) C 14 - C 16	0.32885	21.31	0.28	0.069
BD (2) C 14 - C 16	1.64749	BD*(2) C 9 - C 11	0.3772	21.32	0.28	0.07
BD (2) C 14 - C 16	1.64749	BD*(2) C 10 - C 12	0.29651	18.46	0.29	0.066

Table 4: Theoretical gas phase transitions of the various subsystems 1a-d, using TD-B3LYP/6-311++G(d,p).

Single point vertical excitation	1a	1b	1c	1d	Compound 1
S1	292	274	308	298	326
S2	261	260	285	292	292
S3	239	245	254	282	284

Table 5: Experimental and theoretical UV spectra of compound 1, calculated at TD-B3LYP/6-311++G(d,p).

	Theoretical												Experimental	
E. state	**Gas phase**				**Ethanol**				**Benzene**				**Ethanol**	**Benzene**
	Config.	**Coeff.**	**f**	**λ nm**	**Config.**	**Coeff.**	**F**	**λ nm**	**Config.**	**Coeff.**	**F**	**λ nm**	**λ max, nm**	**λ max, nm**
S1	54 -> 56	0.2085	0.192	326.5	54 -> 56	0.1461	0.352	326.9	54 -> 56	0.14483	0.347	329.4	281	306
	55 -> 56	0.6526			55 -> 56	0.6728			55 -> 56	0.67511				
	55 -> 57	0.1281			55 -> 57	0.1109			55 -> 57	0.1089				
S2	52 -> 56	0.3750	0.141	292.2	52 -> 56	0.1891	0.217	293.4	52 -> 56	0.21648	0.268	294.9		
	53 -> 56	-0.2727			53 -> 56	-0.1520			53 -> 56	-0.14523				
	54 -> 56	0.4875			54 -> 56	0.6262			54 -> 56	0.62199				
	55 -> 56	-0.1533			55 -> 56	-0.1423			55 -> 56	-0.14245				
	55 -> 57	0.1040			55 -> 57	0.1253			55 -> 57	0.11855				
S3	52 -> 56	0.5326	0.204	284.1	52 -> 56	-0.1318	0.222	286.3	52 -> 56	-0.28867	0.218	286.8		
	53 -> 56	-0.1192			53 -> 56	0.6464			53 -> 56	0.58465				
	54 -> 56	-0.3964			54 -> 56	0.1770			54 -> 56	0.21849				
	55 -> 56	0.1594			55 -> 56	-0.1088								
	55 -> 57	-0.1127												

Table 6: Experimental and theoretical UV spectra of compound 2, calculated at TD-B3LYP/6-311++G(d,p).

	Theoretical												Experimental	
E. State	**Gas phase**				**Ethanol**				**Benzene**				**Ethanol**	**Benzene**
	Config.	**Coeff.**	**f**	**λ nm**	**Config.**	**Coeff.**	**F**	**λ nm**	**Config.**	**Coeff.**	**f**	**λ nm**	**λ max, nm**	**λ max, nm**
S1	58 -> 60	0.2331	0.298	327.5	58 -> 60	-0.1386	0.557	330.5	58 -> 60	0.1425	0.541	332.5	336	338
	59 -> 60	0.6445			59 -> 60	0.6786			59 -> 60	0.6781				
	59 -> 61	-0.1358			59 -> 61	0.1066			59 -> 61	-0.1069				
S2	56 -> 60	0.1334	0.347	297.6	58 -> 60	0.6523	0.261	300.4	58 -> 60	0.6553	0.315	301.8	305	307
	57 -> 60	0.1236			59 -> 60	0.1621			59 -> 60	-0.1642				
	58 -> 60	0.6087			59 -> 61	-0.1770			59 -> 61	-0.1606				
	59 -> 60	-0.2500												
	59 -> 61	-0.1571												
S3	56 -> 60	0.4687	0.064	287.7	56 -> 60	0.1596	0.051	289.6	56 -> 60	0.2634	0.054	289.5		
	57 -> 60	0.4718			57 -> 60	0.6575			57 -> 60	0.6220				
	58 -> 60	-0.1779			59 -> 62	0.1374			58 -> 60	-0.1030				
									59 -> 62	-0.1272				

Table 7: Experimental and theoretical UV spectra of 3, calculated at TD-B3LYP/6-311++G(d,p).

	Theoretical												Experimental	
E. state	**Gas phase**				**Ethanol**				**Benzene**				**Ethanol**	**Benzene**
	config	**coefficient**	**f**	**λ nm**	**config**	**coeffici**	**f**	**λ nm**	**config**	**coefficient**	**f**	**λ nm**	**λ max, nm**	**λ max, nm**
S1	62 -> 64	0.1445	0.58	335	63 -> 64	0.6965	0.8	345	63 -> 64	0.1919	0.82	346	**349**	**348**
	63 -> 64	0.6737												
	63 -> 65	-0.1249												
S2	62 -> 64	0.6279	0.13	310	62 -> 64	0.6256	0.05	310	62 -> 64	0.63761	0.07	312		
	63 -> 64	-0.1840			63 -> 65	0.2952			63 -> 65	-0.2677				
	63 -> 65	-0.2414												
S3	61 -> 64	0.2089	0.02	289	61 -> 64	-0.2118	0.03	290	61 -> 64	0.1919	0.04	291		
	62 -> 64	0.2576			62 -> 64	-0.2941			62 -> 64	0.2705				
	63 -> 65	0.6026			63 -> 65	0.5916			63 -> 65	0.6100				

Table 8: Experimental and theoretical UV spectra of compound 4, calculated at TD-B3LYP/6-311++G(d,p).

	Theoretical												Experimental	
E. states	**Gas phase**				**Ethanol**				**Benzene**				**Ethanol**	**Benzene**
	config	**Coeff.**	**f**	**λ nm**	**Config.**	**Coeff.**	**f**	**λ nm**	**Config.**	**Coeff.**	**f**	**λ nm**	**λ max, nm**	**λ max, nm**
S1	62 -> 64	0.2376	0.418	331.4	62 -> 64	0.1615	0.459	334.44	62 -> 64	0.1585	0.466	340.2	298	310
	63 -> 64	0.6451			63 -> 64	0.6740			63 -> 64	0.6752				
	63 -> 65	-0.1248			63 -> 65	0.1032			63 -> 65	0.1020				
S2	60 -> 64	0.1164	0.27	272.4	62 -> 64	0.6599	0.406	272.31	62 -> 64	0.6630	0.433	278.2	270	284
	62 -> 64	0.6269			63 -> 64	-0.1806			63 -> 64	-0.1768				
	63 -> 64	-0.2557			63 -> 65	0.1249			63 -> 65	0.1164				
	63 -> 65	-0.1218												
S3	60 -> 64	0.6395	0.029	245.5	60 -> 64	0.6098	0.024	245.64	60 -> 64	0.6329	0.022	252.5		
	61 -> 64	0.2527			61 -> 64	0.3231			61 -> 64	0.2834				
	62 -> 64	-0.1292												

Table 9: Diffusion coefficient of all studied compounds in ethanol and benzene obtained from MD simulation.

Diffusion coefficient (cm^2/s)		
	Ethanol	**Benzene**
Parent	**$3.84x\ 10^{-5}$**	**$4.23\ x\ 10^{-5}$**
CH_3	**$4.79\ x\ 10^{-5}$**	**$4.98\ x\ 10^{-5}$**
OCH_3	**$6.32\ x\ 10^{-5}$**	**$5.06\ x\ 10^{-5}$**
Cl	**$4.12\ x\ 10^{-5}$**	**$4.43\ x\ 10^{-5}$**

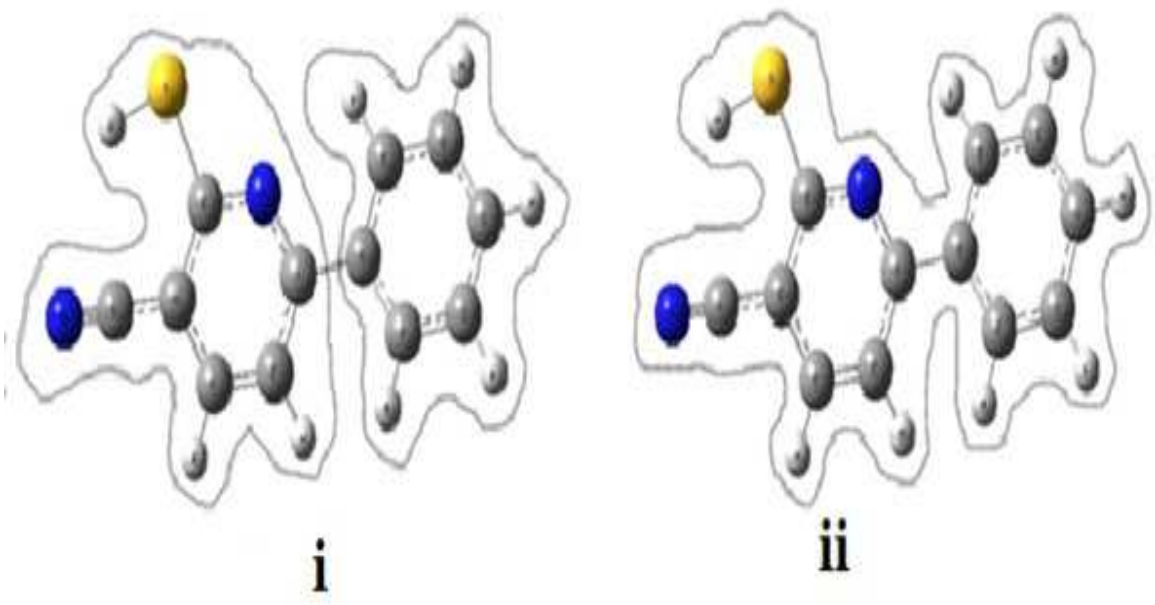

Scheme 2: The two possible types of interaction between subsystems.

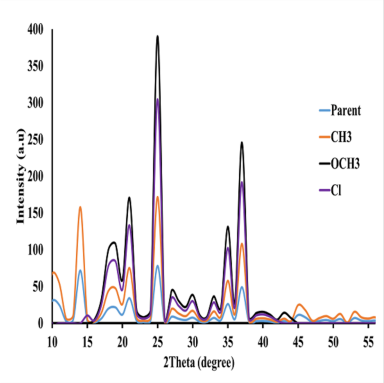

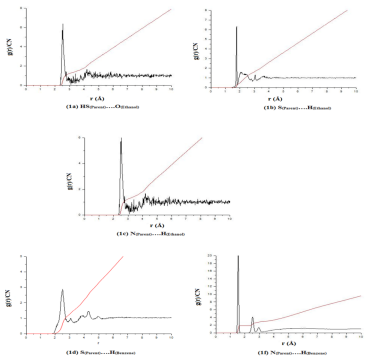

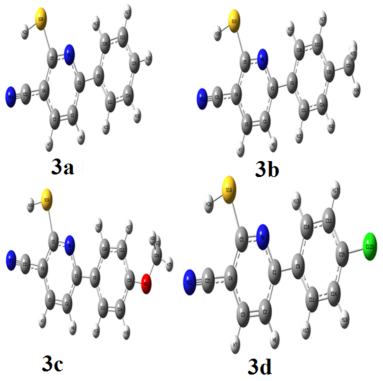

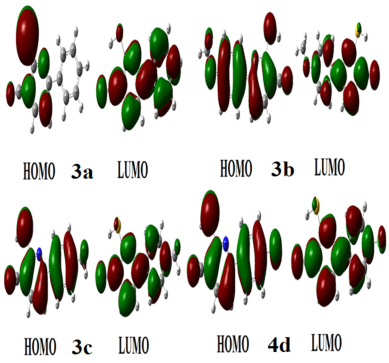

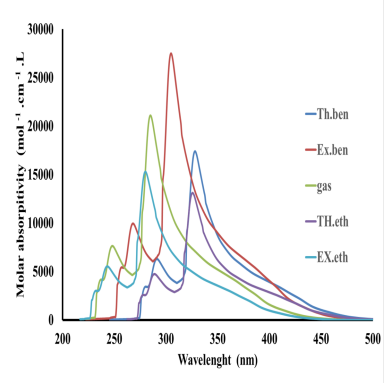

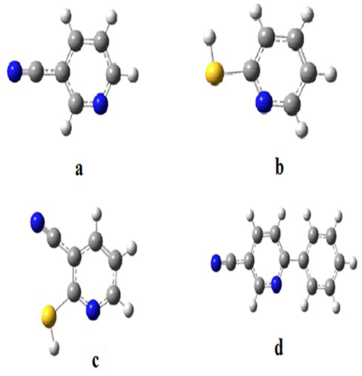

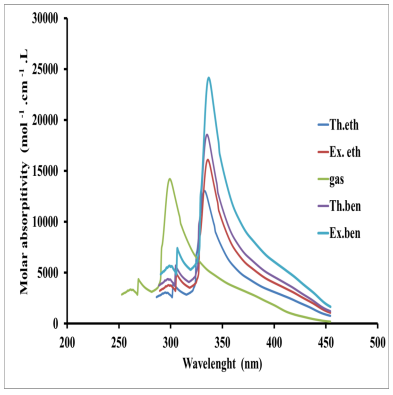

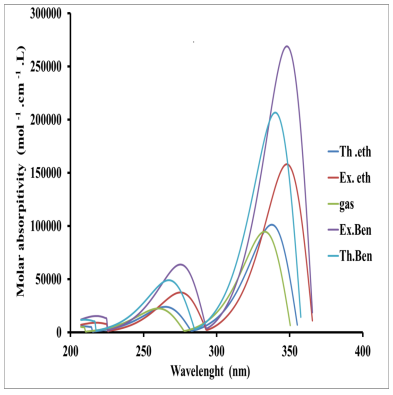

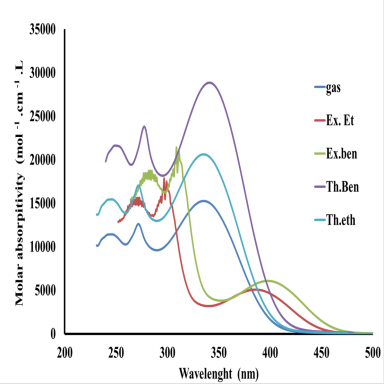

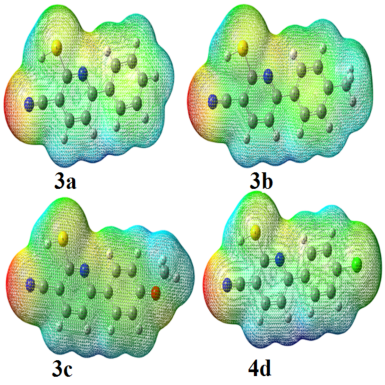

Highlights

1- RDFs, CNs exhibits stronger interactions with ethanol and benzene especially, compounds 3b and 3c.
2- Lowest values of D of Methoxy compound indicated stronger interaction with solvent.
3- Methoxy compound has highest polarity and reactivity.
1- All studied compounds could be used as good candidates for non-linear optics applications.